Optical spike amplitude weighting and neuromimetic rate coding using a joint VCSEL-MRR neuromorphic photonic system

IOP Publishing Neuromorph. Comput. Eng. 4 (2024) 024011 https://doi.org/10.1088/2634-4386/ad4b5b

NEUROMORPHIC
Computing and Engineering

OPEN ACCESS

RECEIVED
18 December 2023

REVISED
17 April 2024

ACCEPTED FOR PUBLICATION
14 May 2024

PUBLISHED
11 June 2024

PAPER

Optical spike amplitude weighting and neuromimetic rate coding using a joint VCSEL-MRR neuromorphic photonic system

Matěj Hejda[1,2,*], **Eli A Doris**[3], **Simon Bilodeau**[3], **Joshua Robertson**[1], **Dafydd Owen-Newns**[1], **Bhavin J Shastri**[4], **Paul R Prucnal**[3] and **Antonio Hurtado**[1]

[1] Institute of Photonics, SUPA Dept of Physics, University of Strathclyde, Glasgow, United Kingdom
[2] Hewlett Packard Labs, Hewlett Packard Enterprise, Hermeslaan 1A, Machelen, Belgium
[3] Department of Electrical and Computer Engineering, Princeton University, Princeton, NJ, United States of America
[4] Department of Physics, Engineering Physics and Astronomy, Kingston, ON, Canada
[*] Author to whom any correspondence should be addressed.

E-mail: matej.hejda@hpe.com and and antonio.hurtado@strath.ac.uk

Keywords: optical computing, VCSEL, microring resonator, vertical cavity surface emitting laser, neuromorphic photonics, photonic spiking neuron

Abstract

Spiking neurons and neural networks constitute a fundamental building block for brain-inspired computing, which is poised to benefit significantly from photonic hardware implementations. In this work, we experimentally investigate an interconnected optical neuromorphic system based on an ultrafast spiking vertical cavity surface emitting laser (VCSEL) neuron and a silicon photonics (SiPh) integrated micro-ring resonator (MRR). We experimentally demonstrate two different functional arrangements of these devices: first, we show that MRR weight banks can be used in conjunction with the spiking VCSEL-neurons to perform amplitude weighting of sub-ns optical spiking signals. Second, we show that a continuously firing VCSEL-neuron can be directly modulated using a locking signal propagated through a single weighting MRR, and we utilise this functionality to perform optical spike firing rate-coding via thermal tuning of the MRR. Given the significant track record of both integrated weight banks and photonic VCSEL-neurons, we believe these results demonstrate the viability of combining these two classes of devices for use in functional neuromorphic photonic systems.

1. Introduction

There is an ever-increasing demand for processing of large, complex datasets that is driven by the exponentially growing amount of available and produced data. Arguably the most advanced data processing capabilities are offered by machine learning (ML) and artificial intelligence (AI) algorithms, driving a massive expansion in scale and complexity of these approaches. While impressive achievements have been demonstrated with large-scale, state-of-the-art AI models, the significant energy requirements and carbon footprint [1] of these computing approaches cannot be neglected. Furthermore, current general purpose digital chip architectures are starting to slowly approach physical limitations in terms of further downscalling, therefore fuelling the exploration of various dedicated, application specific computing architectures.

One of such applications is computation of artificial neural networks (ANNs) which underpin many of modern ML approaches. Driven by the goal of decreasing resource requirements of ML, more focus is also shifting towards spiking neurons and spiking neural networks (SNNs) that more closely resemble their biological counterparts. SNNs represent a third generation of ANNs [2] and rely on sparsely coded, event-based signalling that natively encodes information in time. Furthermore, neuromorphic engineering explores how some of the biological brain's mechanisms can be utilised on hardware level to realise more efficient AI computation. In particular, neuromorphic systems in photonics offer some desirable potential benefits such as low-loss waveguiding, unparalleled bandwidth of photonic systems or very low energy operation [3]. The field of neuromorphic photonics is expanding rapidly, and a wide variety of approaches and photonic devices have been shown to exhibit the desired behaviour and functionalities necessary for

such systems. Optical spiking and excitability with direct applications to spike-based information processing have been demonstrated in phase-change materials [4], micro-ring resonators (MRR) [5], photonic crystals [6], superconducting Josephson junction optoelectronics [7], semiconductor [8] and graphene-based lasers [9], lasers coupled to excitable resonant tunnelling diodes [10, 11], optical modulators [12] and semiconductor optical amplifiers [13].

In this work, we combine two promising systems from the field of neuromorphic photonics: a spiking artificial photonic neuron based upon a vertical cavity surface emitting laser (VCSEL) [14] and a MRR integrated in a silicon photonics (SiPh) platform [15, 16]. While spike weighting in the framework of photonic SNNs has been studied in various theoretical studies [5, 15, 17] or reported experimentally with alternative weighting mechanisms such as using phase-change materials [4] or Mach–Zehnder interferometer meshes [18], experimental demonstration of MRR-based spike weighting for photonic neuromorphic computing has, to the best of our knowledge, not yet been demonstrated. This paper provides an experimental demonstration of two functional layouts using VCSELs together with SiPh MRRs: synaptic spike amplitude weighting of the high-speed (sub-nanosecond long) VCSEL-neuron spiking signals using a single MRR in the weight bank (demonstrating functionality theoretically proposed in [15]), and a spike rate coding mechanism using a continuously (tonic) firing VCSEL-neuron directly controlled with a locking (injection) signal modulated by the MRR. These two different experimental layouts demonstrate how these two systems can cooperate in various ways, achieving useful functionalities for spike-based information processing.

The manuscript is divided as follows: Section 2 introduces the VCSEL and the photonic integrated circuit (PIC) with MRRs used in the experiments and provides their characteristics. In section 3, we describe the experimental setup and achieved results for VCSEL-neuron spike weighting in the MRR. In section 4, we demonstrate spiking rate coding in the VCSEL-neuron with injection power modulation via the weight bank MRR. Finally, discussion and conclusions are provided in section 5.

2. Devices characterisation

In these experiments, we use a telecom-wavelength VCSEL as the spiking photonic neuron. VCSELs have been demonstrated to exhibit a wide range of laser dynamics, with excitable spiking being particularly interesting for the field of neuromorphic engineering. Sub-nanosecond optical spiking regimes can be readily activated [19] and inhibited [20] in injection-locked or electrically-modulated [21] VCSELs to achieve neuron-like spiking dynamics. The VCSEL used in this work operates at the standard telecom wavelength of 1550 nm. Its emission spectrum is shown in figure 1(b) and exhibits two peaks (separated by approximately 250 pm) corresponding to the two orthogonal polarisations of the device's fundamental transverse mode. In this case, the higher wavelength polarisation is dominant while the other remains suppressed (subsidiary mode). Using notation from previous works [22], these two modes can also be referred to as the orthogonal and parallel polarisations of the fundamental mode. The lasing threshold is approx. $I_T \approx 1.5$ mA. The VCSEL is injection locked to a polarisation-matched external CW signal with a small negative frequency detuning Δf. In such an operational regime, amplitude (power) perturbations of the injection signal may elicit sub-ns spiking responses if the perturbation is sufficiently strong (crossing a 'spiking threshold' power value). The spiking responses from the VCSEL-neuron exhibit all the typical hallmarks of excitability such as all-or-nothing character and refractory (lethargic) period with dynamical behaviour analogous to leaky integrate-and-fire neuronal models [23].

Micro-ring resonators [24] form the basis for various PICs, including integrated true time delay banks [25], dense wavelength-division multiplexing transceivers for high-performance computing [26] or optical neuro-synaptic and neural networks [4, 27, 28], among others. The MRR used in this work forms part of a weight bank PIC [16] that incorporates five MRRs and allows for broadcast and weight operation [15]. The MRRs are in the 'add-drop' configuration with adjacent THRU/IN ports connected and adjacent ADD/DROP ports connected. This weight bank is on a chip fabricated by Advanced Micro Foundry in a multi-project wafer run coordinated by CMC Microsystems. A micrograph of the MRR weight bank PIC is shown in figure 1(a). The core layer is 220 nm nm thick Si, with 500 nm wide bus and ring waveguides. Separation between the coupling bus waveguide and the ring waveguide is 200 nm and the five MRRs have radii around 8 μm varied slightly to produce approximately 1 nm resonance spacing. From the weight bank, a single MRR is selected whose resonance provides a closest (approximate) wavelength match to the emission wavelength of the VCSEL. The DROP and THRU port spectra of this weight bank are shown in figures 2(a) and (d), highlighting the tuning ranges of MRR resonances (gray regions) along with a fixed resonance of another MRR in the weight bank. As expected, the lack of change in resonance of the non-actuated MRR during selected MRR tuning indicates low cross-talk and independent MRR operation. Figure 2 also shows the expected power at a given, fixed wavelength (highlighted by a dashed red line, figures 2(c) and (f)) and

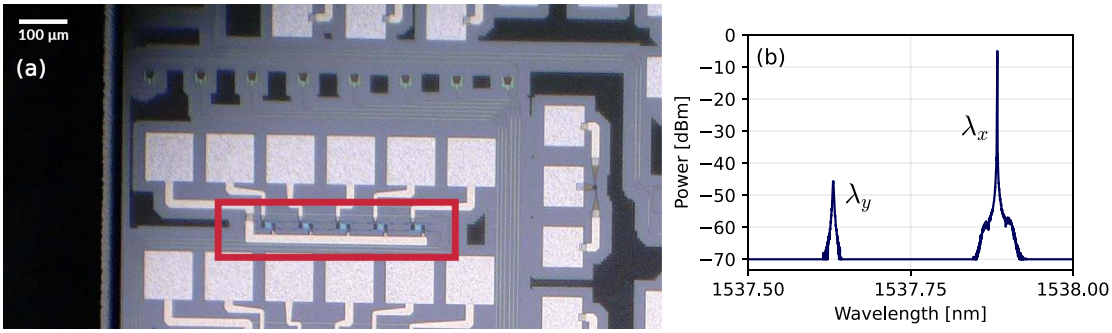

Figure 1. (a) Micrographs of the PIC chip, with five MRRs of the photonic weight bank highlighted in red. (b) Optical spectrum of a free-running 1550 nm VCSEL used in this work. The spectrum exhibits two peaks: a dominant (λ_x) and subsidiary (λ_y) peak. These correspond to the mutually orthogonal polarisations of the fundamental lasing mode.

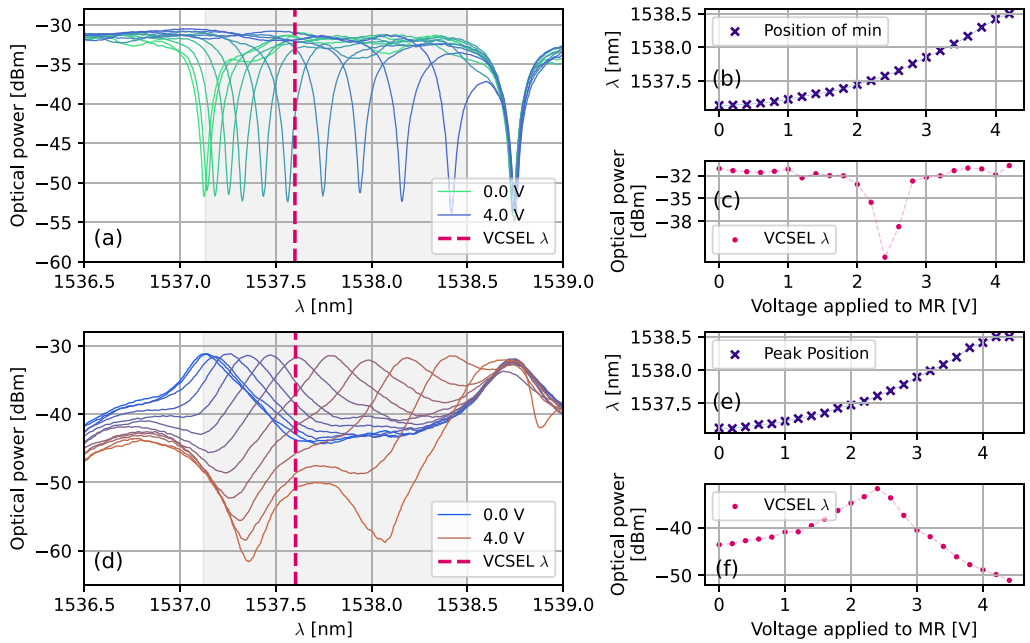

Figure 2. Selected MRR characterisation. (a) THRU port readout during V_{MR} sweep, (b) position of resonance as a function of applied bias V_{MR}, (c) detected optical power through the THRU port at a selected fixed wavelength (dashed line in (a)); (d) DROP port readout during V_{MR} sweep, (e) position of resonance as a function of applied bias V_{MR}, (f) detected optical power through the DROP port at a selected fixed wavelength (dashed line in (d)).

the position of the actuated MRR resonance as a function of the bias voltage V_{MR} applied to the MRR heater element (figures 2(b) and (e)) . We also want to mention that the MRR detuning is plotted with respect to bias voltage (rather than power) applied to the MRR heater.

3. Post-neuronal weighting: VCSEL → MRR

First, we investigate the viability of the integrated MRR as part of a photonic weight bank to controllably weight the amplitude of optical spiking signals delivered by a VCSEL-neuron. The sub-ns spikes to be weighted were deterministically elicited in the VCSEL when subject to the injection of externally modulated light signal [22]. Afterwards, the output spiking signals were coupled to the PIC, where a single MRR was used to alter the signal (spike) amplitude via MRR resonance adjustment using a ring heater.

3.1. Methods

The experimental setup for the VCSEL-to-MRR system is shown in figure 3(a). The optical injection into the VCSEL neuron is performed using an external tuneable laser (EMCORE micro-ITLA). Prior to entering the VCSEL, the injection lane was split with a 90:10 optic splitter, with the 10% branch used for injection power monitoring. The 90% power branch is fed into the VCSEL through a circulator, which also allows to obtain the VCSEL's output signal. The VCSEL was biased at 5 mA (above the lasing threshold of 1.5 mA), which

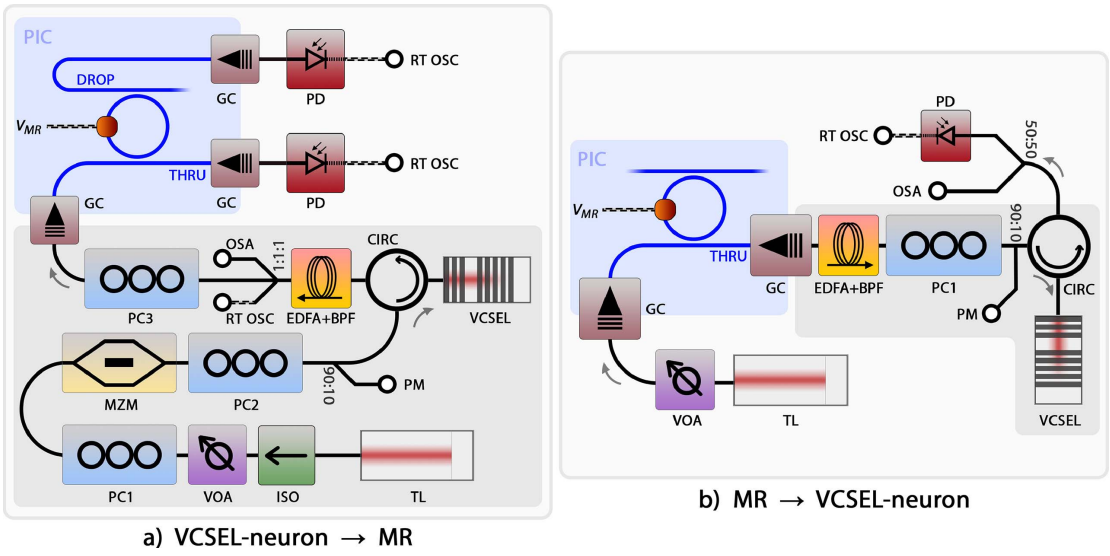

Figure 3. Experimental setups for (a) spike weighting in the MRR, and (b) direct VCSEL modulation via signal coming through a MRR. TL—tuneable laser; ISO—isolator; VOA—variable optical attenuator; PC(1,2,3)—polarisation controllers; MZM—Mach–Zehnder modulators; PM—power meter; CIRC—circulator; VCSEL—vertical cavity surface emitting laser; EDFA—erbium-doped fibre amplifier; BPF—bandpass filter; RT OSC—real-time oscilloscope; OSA—optical spectrum analyser; GC—grating coupler; PD—photodetector. Ratios indicated are for the power couplers/splitters.

corresponds to optical output power of a free-running device $P_{\mathrm{VCSEL}} = 390\,\mu$W. The injection detuning was approx. -3 GHz with respect to the orthogonally-polarised mode of the device and the injection line power was 170 μW. The VCSEL output (collected from the third port of the optical circulator) was then amplified using an erbium-doped fibre amplifier (EDFA; PriTel) and equally split using a 1-to-4 fibre splitter (Thorlabs). These outputs were used to provide the signal into the SiPh chip, as well as to directly monitor the VCSEL output time trace via a photodetector and a 33 GHz real-time oscilloscope (PD, RT OSC; Discovery Semiconductors Lab Buddy, Tektronix MSO/DPO70000) and the VCSEL's optical spectrum using an optical spectrum (OSA; Apex Technologies). The VCSEL output was coupled to the chip via foundry-provided grating couplers optimised for 1550 nm light under an incident angle of 8 degrees. An 8-fibre V-groove array polished at 8 degrees, manufactured by OZ Optics, was positioned above an array of 8 grating couplers on the chip. The first and last grating couplers are directly connected with a loopback waveguide, allowing for optical alignment and loss measurement by monitoring a constant-power alignment signal. An input signal of 10 dBm was injected into the alignment port, and a power of approximately -3 dBm was measured at optimal alignment . This indicates a loss per grating coupler of approximately 6–7 dBm, which is typical for such structures in practical use.

During this experiment, the injection-locked spiking VCSEL neuron was continuously triggered with a sequence of repeated perturbations modulating the injection. The modulation signal for the optical injection line was generated on an arbitrary waveform generator (AWG; Tektronix AWG7122B, 12 GSa s^{-1}) and realised using a fibre optic Mach–Zehnder modulator (MZM). This RF modulation signal had a form of return-to-zero square pulses of 667 ps (8 Sa) with 4.66 ns (8×7 Sa) spacing, using peak-to-peak DAC range of 600 mV in the AWG. For each of these pulses, a single optical sub-ns spike was deterministically elicited at the VCSEL output. To perform the weighting, the selected MRR on the SiPh chip was swept through a range of DC voltages V_{MR} applied to the ring heater element.

3.2. Results

For each bias V_{MR} applied to the MRR heater, a time trace with $n_s = 7$ spikes was acquired. In total, 29 voltage steps were recorded, from $V_{\mathrm{MR}} = 1$ V to 3.9 V with 100 mV increments. This sweep was repeated $n_m = 15$ times for statistical evaluation. In each case, traces were recorded from: (1) the direct VCSEL output, (2) the THRU port of the MRR, and (3) the DROP port of the MRR. All time traces collected from the THRU port of the MRR are shown in red, and all the traces collected from the DROP port are shown in green. For each V_{MR} during each of these $n_m = 15$ repeated acquisition, the amplitude of each single obtained (MRR-weighted) spike was analysed individually. The maximum (spike peak) was located, and using the position of this spike peak as an alignment reference, all the spike traces were aligned. An average over all the aligned time traces is calculated, yielding a representative weighted spike for a given V_{MR} from all the

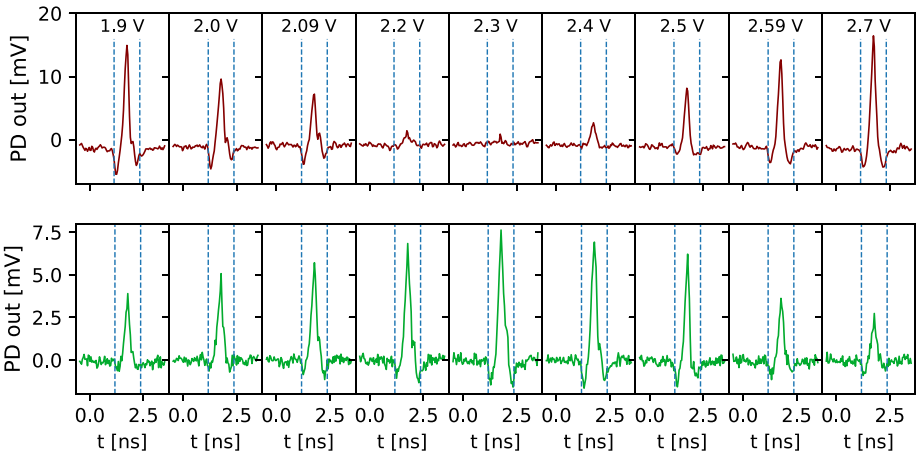

Figure 4. Demonstration of spike amplitude weighting at both THRU (top row) and DROP (bottom row) ports of the MRR output. In each case, the spike trace shown corresponds to a mean spike envelope calculated from all the recorded repetitions for a given value of V_{MR}.

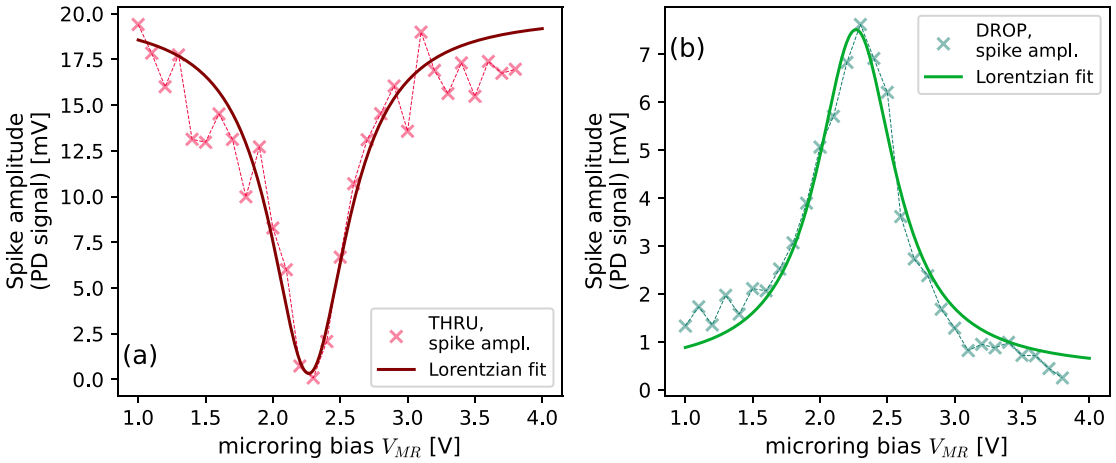

Figure 5. Mean amplitudes of all spikes ($n_s = 7$ per measurement, $n_m = 15$ repetitions) as a function of MRR heater bias voltage V_{MR} with a Lorenzian fit (solid line) using the least squares method. The two plots show (a) THRU; (b) DROP port readouts.

repeated measurements. Thanks to the spike peak alignment for the averaging procedure, issues coming from small trace misalignment or jittering are avoided. These mean representative spikes are shown in figure 4.

After calculating the representative spike, its maximum is saved as the representative spike amplitude. The same procedure was followed for both the DROP and THRU ports of the MRR. The resulting representative peak spike amplitudes are shown in figures 5(a) and (b). Both figures were fitted with a Lorentzian in the interval around the extrema, showing a good degree of agreement in this range of MRR heater bias voltages. Following a previously reported methodology [29], an estimate of the total dynamic range of the spike amplitude weighting process was calculated from the maximum achieved mean spike amplitude minus the noise floor (RMS), and equals to $\mathrm{DR_{THRU}} = 17.05$ dB (or bit resolution of ≈5.7 bit) and $\mathrm{DR_{DROP}} = 14.49$ dB (or bit resolution of ≈4.9 bit). It is worth noting that the y-axis in figure 5 is linear, unlike in figure 2 where it is logarithmic. The THRU photodetector time traces did not contain the DC signal component (constant lasing emission from the VCSEL operated above the threshold). Therefore, this DC component was also numerically filtered from the DROP port signal to compare signals of equivalent nature.

4. Pre-neuronal modulation: MRR → VCSEL

In this second demonstration, we injection lock the VCSEL to a CW signal passing through a single MRR in the integrated weight bank to realise a spiking VCSEL-neuron. By directly modulating the constant locking signal via MRR (changing its power), we introduce continuous spiking dynamics in the VCSEL-neuron, where the spike firing frequency is inversely proportional to the input power [30]. The capability of VCSELs to directly encode analog signals into continuous, real-time encoded spike trains that represent input signal

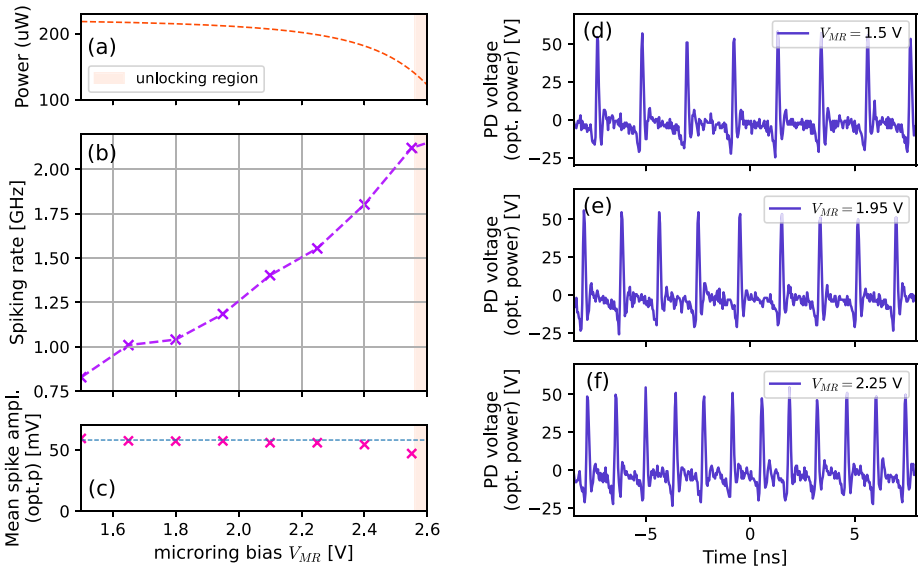

Figure 6. Demonstration of rate coding in spiking VCSEL-neuron injection locked to a signal coming from the MRR. (a) Injection signal power as a function of V_{MR}. (b) Spike firing rate in the VCSEL-neuron as a function of V_{MR}. (c) Mean spike amplitudes within the spike train. (d)–(f) Examples of continuous spiking traces produced by the VCSEL-neuron locked to the signal from the MRR. As the voltage applied to the MRR heater is gradually increased from (d) 1.5 V through (e) 1.95 V to (f) 2.25 V, the spike firing rate monotonically increases.

amplitude in the local spike firing rate [30] holds promise for utilizing VCSELs as optical spike-domain input encoders. This functionality was previously demonstrated on multichannel (RGB) digital images [31] using a time-domain multiplexed, implementation-friendly single VCSEL-neuron layout.

4.1. Methods

The experimental setup for the MRR-to-VCSEL system is shown in figure 3(b). To realise the direct injection locking of the VCSEL to a signal modulated using the MRR on the SiPh chip, a CW signal from the tunable laser (EMCORE micro-ITLA) was passed through a variable optical attenuator and coupled to the PIC using the same approach as previously described. The THRU port of this MRR was then coupled off the chip into a fibre. After the MRR-modulated signal was collected from the chip, it was amplified via an EDFA (with a bandpass filter) and injected into the VCSEL through a polarisation controller and a circulator, with injection power $P_{\mathrm{inj}} \approx 220\,\mu$W. This CW signal was polarisation adjusted to ensure locking into the orthogonal (dominant) polarisation, and wavelength adjusted to ensure injection detuning of approximately -3.75 GHz. The output of the VCSEL-neuron was then collected through the circulator and recorded using an amplified photodetector (Discovery Semi LabBuddy) on a real-time oscilloscope (RT OSC).

4.2. Results

The MRR-to-VCSEL experiment results are shown in figure 6. A sweep of the MRR heater bias voltage V_{MR} was performed from 1.5 V to 4.5 V with 150 mV increments (total of 21 measurements). For each V_{MR}, a 40 ns trace was acquired, where individual spikes were counted and related to the recording length ($t_{\mathrm{len}} = 40$ ns) to obtain the local spiking rate. This procedure was repeated $n = 12$ times, yielding the representative mean firing rate (and its dependence on applied MRR heater bias V_{MR}).

The optical power of the locking signal to the VCSEL as a function of V_{MR} is shown in figure 6(a). As the resonance of the MRR shifts during the V_{MR} sweep towards the wavelength of the locking signal, the optical power present at the THRU port of the MRR decreases. In the injection locked layout used for the VCSEL-neuron, this means weakening of the locking signal. For a VCSEL in a continuously firing regime, this increases the spiking frequency [30]. This is demonstrated in figure 6(b) by the monotonically increasing spike firing rate. Under the given set of experimental conditions at the start of the experiment (with the MRR resonance frequency far from the locking signal frequency), the VCSEL-neuron fires continuously with a mean spiking rate of ≈750 MHz that increases towards ≈2.25 GHz, which approximately represents the highest achievable spike firing rate in this VCSEL, in this case achieved for $V_{\mathrm{MR}} = 2.55$ V. The spike firing rate modulation effect is also demonstrated by examples of VCSEL-neuron output traces for different values of V_{MR} shown in figures 6(d)–(f).

By further increasing the MRR bias, the power at the THRU port drops significantly as the ring resonance is approached. In the VCSEL-neuron, for such a significant reduction of input injection power, we have

observed a gradual transition from continuous, distinct repeated spikes to period-1 resembling dynamics with a noticeable lowering of oscillation amplitude, followed by breaking of injection locking and the oscillation-like dynamics. This is shown in figure 6(c) as a sudden decrease in recorded mean spike amplitude. For such low levels of injected signal, the injection locking of the VCSEL-neuron is (temporarily) broken, and the VCSEL starts behaving as a free-running laser without exhibiting spiking dynamics. Therefore, to realise rate-coding in the VCSEL-neuron using this layout, only a part of the ring's dynamical range should be used to avoid unlocking when the MRR resonance aligns too closely with the locking signal.

5. Discussion and conclusions

This work provides the first experimental demonstration of interconnectivity between spiking photonic VCSEL-neurons and integrated MRR weight banks, with a focus on two key relevant functions for future scaled-up photonic neural computing: spike weighting and all-optical rate-encoding. In both of these cases, the MRR is utilised as a programmable optical attenuation element at a given wavelength matched to that of the VCSEL-based spiking neuron. Other integrated devices, such as MZMs, could also be utilised for this purpose, with discrete MZMs being used extensively in previous -based spiking VCSEL implementations [22]. We have selected MRRs for this experimental study due to their wavelength-selective nature that matches well the need to injection lock the VCSEL to achieve spiking operation, and which allows to perform the required controllable frequency detuning directly within the MRR. Furthermore, MRRs are suitable for operation with wavelength-division multiplexed (WDM) signals, which goes beyond the scope of this study but represents a desirable solution for networks with multiple independent photonic neurons operating each at different wavelengths. MRRs also typically have smaller chip footprint than MZMs, which is desirable for achieving higher integration density, and calibration protocols for MRR weight banks have been previously reported [29], allowing for optimised operation of MRR-based optical neural networks. A hypothetical WDM-based optical neural network would directly allow for fan-out (signal from one VCSEL weighted through multiple MRRs), a fan-in through optoelectronic conversion and direct VCSEL modulation [32] or through selective locking of the VCSEL to distinct WDM channels.

In the current first iteration of these functional layouts, both were realised using a commercially sourced, telecom-wavelength, fibre-coupled off-chip VCSEL coupled to the PIC incorporating the MRR (weight bank) via grating couplers. Alternatively, edge-couplers could also be utilised [33, 34], although these are typically very sensitive to misalignment and facet quality. While coupling of the off-chip laser allows for additional flexibility and control when realizing the experiments, the ultimate goal lies in a system that is packaged or realised fully on-chip, therefore integrating more tightly the spiking VCSELs with integrated photonic circuits. Such approach would allow to create more scalable systems that are also more robust to environment-induced noise. This requires removing as many bulky off-chip components as possible (e.g. EDFAs, polarisation controllers, circulators) as well as minimising optical coupling hardware (i.e. removing the need for 6-DOF mechanical alignment stages).

The first packaging miniaturisation step could be to move from coupling to photonic wire bonding [35] where short, freeform 3D printed waveguides would couple light between the VCSEL and the silicon. This would introduce a more stable and low-loss coupling, both with respect to power and polarisation. Photonic wire bonds are typically fabricated by means of two-photon polymerisation [36] and have been shown to provide down to sub-1 dB insertion loss [37, 38], which should allow operation with typical optical power levels of VCSELs and mitigate the need for EDFAs for injection locking and cascading of photonic neurons. Additionally, since the length of the waveguide would be extremely short (microns) compared to typical lengths of optical fibre (tens of centimetres to metres), very little polarisation drift due to birefringence would be expected. This would eliminate the need for off-chip polarisation control, although it comes with the caveat that on-chip polarisation and polarisation components [39] tend to be limited to strictly-TE or strictly-TM modes due to high intrinsic waveguide birefringence.

An additional challenge towards miniaturisation is in the general lack of straightforward foundry-standard methods to do non-reciprocal optics (i.e. circulators and isolators). The most popular approaches to isolation/circulation involve magneto-optic materials [40–43], which are not foundry-standard and therefore incur large additional costs; nonlinear optics [44–46], which generally require high power to function; or modulation-based approaches [47, 48], which require significant amounts of chip area and external modulation/control hardware. In order to circumvent this, the proposed solution for silicon-photonics-friendly VCSEL injection locking is presented in figure 7. Assuming that each VCSEL's primary polarisation is aligned with the TE mode of the waveguide, injected perturbations to induce spiking can be received in the TM mode of the waveguide (which is also the secondary polarisation of the VCSEL).

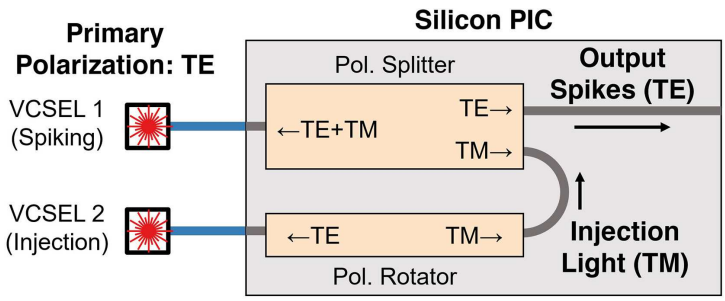

Figure 7. Block diagram for a proposed isolation-free integrated approach to combining spiking VCSELs with a silicon PIC. VCSELs are photonically wire bonded to the PIC such that their primary emission polarisation is aligned with the TE mode of the PIC. A polarisation rotator and splitter allow light from VCSEL 2 to be injected into the secondary polarisation of VCSEL 1 (neuron) in order to add perturbations and create spikes. Output spikes from VCSEL 1 will be emitted with the primary polarisation, which will couple to the TE mode of the PIC and exit from the polarisation splitter into the rest of the PIC.

Furthermore, assuming that polarisation cross-talk of the on-chip components is sufficiently minimal, this will provide an isolation-free method for performing injection locked spiking in the manner presented in this paper.

In conclusion, we have experimentally demonstrated the joint operation of a spiking VCSEL-neuron and a single MRR from an integrated photonic weight bank for operation in all-optical, spike-based information processing. A spike weighting layout (VCSEL-to-MRR) and a direct rate-encoding (MRR-to-VCSEL) layout have been validated, demonstrating both the systems as being mutually compatible and viable building blocks for larger, hybrid photonic spiking networks with sub-ns spike times. This work opens new routes towards novel, more advanced solutions for fully on-chip layouts combining lasers as spiking neurons and integrated weight banks for future functional neuromorphic computing photonic hardware.

Data availability statement

The data that support the findings of this study are openly available at the following URL/DOI: https://doi.org/10.15129/042ffe01-ae5b-4d4e-9d22-580e4d05099b [49].

Acknowledgments

The authors acknowledge support from the European Commission (Grant 828841-ChipAIH2020-FETOPEN-2018-2020) and by the UK Research and Innovation (UKRI) Turing AI Acceleration Fellowships Program 4-(EP/V025198/1). S Bilodeau acknowledges funding from the Fonds de recherche du Québec-Nature et technologies. B Shastri acknowledges funding from the Natural Sciences and Engineering Research Council of Canada (NSERC).

Conflict of interest

The authors declare no conflicts of interest.

ORCID iDs

Matěj Hejda https://orcid.org/0000-0003-4493-9426
Eli A Doris https://orcid.org/0000-0003-4015-3303
Simon Bilodeau https://orcid.org/0000-0003-0667-2732
Joshua Robertson https://orcid.org/0000-0001-6316-5265
Dafydd Owen-Newns https://orcid.org/0000-0001-6592-8465
Bhavin J Shastri https://orcid.org/0000-0001-5040-8248
Antonio Hurtado https://orcid.org/0000-0002-4448-9034

References

[1] Strubell E, Ganesh A and McCallum A 2019 Energy and policy considerations for deep learning in NLP (arXiv:1906.02243)
[2] Maass W 1997 Networks of spiking neurons: the third generation of neural network models *Neural Netw.* **10** 1659–71
[3] Miller D A B 2017 Attojoule optoelectronics for low-energy information processing and communications *J. Lightwave Technol.* **35** 346–96

[4] Feldmann J, Youngblood N, Wright C D, Bhaskaran H and Pernice W H P 2019 All-optical spiking neurosynaptic networks with self-learning capabilities *Nature* **569** 208–14
[5] Han Y, Xiang S, Zhang Y, Gao S, Wen A and Hao Y 2022 An all-MRR-based photonic spiking neural network for spike sequence learning *Photonics* **9** 120
[6] Laporte F, Katumba A, Dambre J and Bienstman P 2018 Numerical demonstration of neuromorphic computing with photonic crystal cavities *Opt. Express* **26** 7955
[7] Shainline J M, Buckley S M, Mirin R P and Nam S W 2017 Superconducting optoelectronic circuits for neuromorphic computing *Phys. Rev. Appl.* **7** 034013
[8] Nahmias M A, Tait A N, Shastri B J, de Lima T F and Prucnal P R 2015 Excitable laser processing network node in hybrid silicon: analysis and simulation *Opt. Express* **23** 26800
[9] Jha A, Huang C, Peng H-T, Shastri B J and Prucnal P 2022 Photonic spiking neural networks and graphene-on-silicon spiking neurons *J. Lightwave Technol.* **40** 1
[10] Ortega-Piwonka I, Hejda M, Alanis J A, Lourenço J, Hurtado A, Figueiredo J M L, Romeira B and Javaloyes J 2022 Spike propagation in a nanolaser-based optoelectronic neuron *Opt. Mater. Express* **12** 2679
[11] Hejda M, Alanis J A, Ortega-Piwonka I, Lourenço J, Figueiredo J, Javaloyes J, Romeira B and Hurtado A 2022 Resonant tunneling diode nano-optoelectronic excitable nodes for neuromorphic spike-based information processing *Phys. Rev. Appl.* **17** 024072
[12] Mourgias-Alexandris G, Totovic A, Tsakyridis A, Passalis N, Vyrsokinos K, Tefas A and Pleros N 2020 Neuromorphic photonics with coherent linear neurons using dual-IQ modulation cells *J. Lightwave Technol.* **38** 811–9
[13] Shi B, Calabretta N and Stabile R 2020 Deep neural network through an InP SOA-based photonic integrated cross-connect *IEEE J. Sel. Top. Quantum Electron.* **26** 1–11
[14] Skalli A, Robertson J, Owen-Newns D, Hejda M, Porte X, Reitzenstein S, Hurtado A and Brunner D 2022 Photonic neuromorphic computing using vertical cavity semiconductor lasers *Opt. Mater. Express* **12** 2395
[15] Tait A N, Nahmias M A, Shastri B J and Prucnal P R 2014 Broadcast and weight: an integrated network for scalable photonic spike processing *J. Lightwave Technol.* **32** 4029–41
[16] Tait A N, de Lima T F, Zhou E, Wu A X, Nahmias M A, Shastri B J and Prucnal P R 2017 Neuromorphic photonic networks using silicon photonic weight banks *Sci. Rep.* **7** 7430
[17] Zhang Y N, Xiang S Y, Han Y N, Guo X X, Zhang Y H, Shi Y C and Hao Y 2023 Supervised learning and pattern recognition in photonic spiking neural networks based on MRR and phase-change materials *Opt. Commun.* **549** 129870
[18] Srouji L E, Lee Y-J, On M B, Zhang L and Yoo S J B 2023 Scalable nanophotonic-electronic spiking neural networks *IEEE J. Sel. Top. Quantum Electron.* **29** 1–13
[19] Hurtado A, Henning I D and Adams M J 2010 Optical neuron using polarisation switching in a 1550nm-VCSEL *Opt. Express* **18** 25170–6
[20] Robertson J, Deng T, Javaloyes J and Hurtado A 2017 Controlled inhibition of spiking dynamics in VCSELs for neuromorphic photonics: theory and experiments *Opt. Lett.* **42** 1560
[21] Robertson J, Wade E and Hurtado A 2019 Electrically controlled neuron-like spiking regimes in vertical-cavity surface-emitting lasers at ultrafast rates *IEEE J. Sel. Top. Quantum Electron.* **25** 1–7
[22] Robertson J, Wade E, Kopp Y, Bueno J and Hurtado A 2020 Toward neuromorphic photonic networks of ultrafast spiking laser neurons *IEEE J. Sel. Top. Quantum Electron.* **26** 1–15
[23] Robertson J, Hejda M, Bueno J and Hurtado A 2020 Ultrafast optical integration and pattern classification for neuromorphic photonics based on spiking VCSEL neurons *Sci. Rep.* **10** 6098
[24] Bogaerts W, De Heyn P, Van Vaerenbergh T, De Vos K, Kumar Selvaraja S, Claes T, Dumon P, Bienstman P, Van Thourhout D and Baets R 2012 Silicon microring resonators *Laser Photon. Rev.* **6** 47–73
[25] Xiang C, Davenport M L, Khurgin J B, Morton P A and Bowers J E 2018 Low-loss continuously tunable optical true time delay based on Si3N4 ring resonators *IEEE J. Sel. Top. Quantum Electron.* **24** 1–9
[26] Liang D *et al* 2020 An energy-efficient and bandwidth-scalable DWDM heterogeneous silicon photonics integration platform *IEEE J. Quantum Electron.* **28** 6100819
[27] de Lima T F *et al* 2019 Machine learning with neuromorphic photonics *J. Lightwave Technol.* **37** 1515–34
[28] Huang C *et al* 2021 A silicon photonic–electronic neural network for fibre nonlinearity compensation *Nat. Electron.* **4** 837–44
[29] Tait A N, de Lima T F, Nahmias M A, Shastri B J and Prucnal P R 2016 Continuous calibration of microring weights for analog optical networks *IEEE Photonics Technol. Lett.* **28** 887–90
[30] Hejda M, Robertson J, Bueno J and Hurtado A 2020 Spike-based information encoding in vertical cavity surface emitting lasers for neuromorphic photonic systems *J. Phys. Photon.* **2** 044001
[31] Hejda M, Robertson J, Bueno J, Alanis J A and Hurtado A 2021 Neuromorphic encoding of image pixel data into rate-coded optical spike trains with a photonic VCSEL-neuron *APL Photon.* **6** 060802
[32] Lee Y-J, On M B, Xiao X, Proietti R and Yoo S J B 2022 Photonic spiking neural networks with event-driven femtojoule optoelectronic neurons based on Izhikevich-inspired model *Opt. Express* **30** 19360
[33] Fang N, Yang Z, Wu A, Chen J, Zhang M, Zou S and Wang X 2009 Three-dimensional tapered spot-size converter based on (111) silicon-on-insulator *IEEE Photonics Technol. Lett.* **21** 820–2
[34] Pu M, Liu L, Ou H, Yvind K and Hvam J M 2010 Ultra-low-loss inverted taper coupler for silicon-on-insulator ridge waveguide *Opt. Commun.* **283** 3678–82
[35] Lindenmann N, Balthasar G, Hillerkuss D, Schmogrow R, Jordan M, Leuthold J, Freude W and Koos C 2012 Photonic wire bonding: a novel concept for chip-scale interconnects *Opt. Express* **20** 17667–77
[36] Adão R M R, Alves T L, Maibohm C, Romeira B and Nieder J B 2022 Two-photon polymerization simulation and fabrication of 3D microprinted suspended waveguides for on-chip optical interconnects *Opt. Express* **30** 9623
[37] Billah M R *et al* 2018 Hybrid integration of silicon photonics circuits and InP lasers by photonic wire bonding *Optica* **5** 876–83
[38] Blaicher M *et al* 2020 Hybrid multi-chip assembly of optical communication engines by *in situ* 3D nano-lithography *Light Sci. Appl.* **9** 71
[39] Sacher W D, Barwicz T, Taylor B J F and Poon J K S 2014 Polarization rotator-splitters in standard active silicon photonics platforms *Opt. Express* **22** 3777
[40] Mitsuya K, Shoji Y and Mizumoto T 2013 Demonstration of a silicon waveguide optical circulator *IEEE Photonics Technol. Lett.* **25** 721–3
[41] Shoji Y and Mizumoto T 2014 Magneto-optical non-reciprocal devices in silicon photonics *Sci. Technol. Adv. Mater.* **15** 014602

[42] Firby C J, Chang P, Helmy A S and Elezzabi A Y 2018 Versatile broadband polarization-independent optical circulators for nanophotonic integrated circuits *J. Opt. Soc. Am.* B **35** 1504
[43] Huang D, Pintus P and Bowers J E 2018 Towards heterogeneous integration of optical isolators and circulators with lasers on silicon [Invited] *Opt. Mater. Express* **8** 2471
[44] Ding M *et al* 2022 Silicon nonlinear switch as a conditional circulator for monostatic LiDAR systems *Photon. Res.* **10** 426
[45] Del Bino L, Silver J M, Woodley M T M, Stebbings S L, Zhao X and Del'Haye P 2018 Microresonator isolators and circulators based on the intrinsic nonreciprocity of the Kerr effect *Optica* **5** 279
[46] Li A and Bogaerts W 2020 Reconfigurable nonlinear nonreciprocal transmission in a silicon photonic integrated circuit *Optica* **7** 7
[47] Doerr C R, Chen L and Vermeulen D 2014 Silicon photonics broadband modulation-based isolator *Opt. Express* **22** 4493
[48] Yu Z and Fan S 2009 Complete optical isolation created by indirect interband photonic transitions *Nat. Photon.* **3** 91–94
[49] Hejda M, Robertson J, Owen-Newns D and Hurtado A 2024 Optical spike amplitude weighting and neuromimetic rate coding using a joint VCSEL-MRR neuromorphic photonic system (University of Strathclyde KnowledgeBase) (https://doi.org/10.15129/042ffe01-ae5b-4d4e-9d22-580e4d05099b)